# LANGMUIR

pubs.acs.org/Langmuir Article

# Controlling the Spatiotemporal Transport of Particles in Fluid-Filled Microchambers

Abhrajit Laskar, Oleg E. Shklyaev, and Anna C. Balazs\*



Cite This: Langmuir 2020, 36, 7124-7132



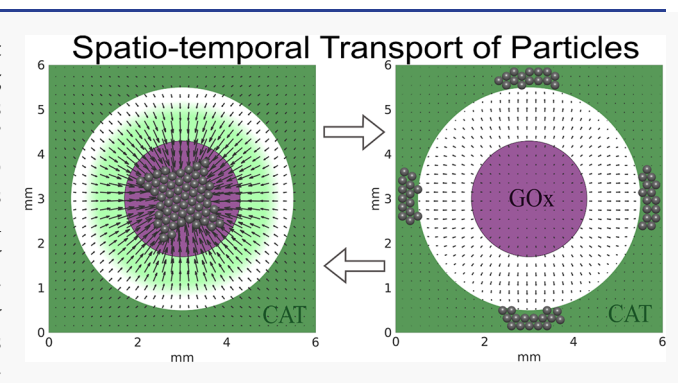
**ACCESS** 

III Metrics & More

Article Recommendations

Supporting Information

ABSTRACT: The development of microscale devices that autonomously perform multistep processes is vital to advancing the use of microfluidics in industrial applications. Such advances can potentially be achieved through the use of "chemical pumps" that transduce the energy from inherent catalytic reactions into fluid flow within microchambers, without the need for extraneous external equipment. Using computational modeling, we focus on arrangements of multiple chemical pumps that are formed by anchoring patches of different enzymes onto the floor of a fluid-filled chamber. With the addition of the appropriate reactants, only one of the enzymatic patches is activated and thereby generates fluid flow centered about that patch. These flows drive the self-



assembly of microparticles in the solution and localize the particles onto the activated patches. By varying the spatial arrangement of the enzymatic patches, and the sequence in which the appropriate reactants are added to the solution, we realize spatiotemporal control over the fluid flow and the sequential transport of microparticles from one patch to another. The order in which the particles visit the different patches can be altered by varying the sequence in which the reactants are added to the solution. By harnessing catalytic cascade reactions, where the product of one reaction is the reactant for the next, we achieve directed transport between the patches with the addition of just one reactant, which initiates the catalytic cascade. Through these studies, we show how the trajectory of the particles' motion among different "stations" can be readily regulated through intrinsic catalytic reactions and thus, provide guidelines for creating fluidic devices that perform multistep reactions in an autonomous, self-sustained manner.

# ■ INTRODUCTION

The chemical industry is undergoing an increasingly rapid transition away from large scale manufacturing plants to microscale fluidic devices for processing operations. With this scaling down, researchers are striving to design devices that are portable and autonomously perform multistep chemical processes, without extraneous mechanical or electrical equipment. The recent advent of "chemical pumps" provides one route to creating microfluidic that perform in an autonomous, self-sustained manner. 1-5 Specifically, Sengupta et al. 2 showed that enzymatic reactions at the surface of a fluid-filled microchamber drive the spontaneous flow of the fluid, and in this manner, the enzymes act as "chemical pumps". Moreover, the chemically generated flows can transport microparticles to specific locations in the chamber.<sup>6,7</sup> These findings pave the way for creating fluidic "microfoundries" that autonomously direct the assembly of particles and the formation of complex microstructures. To further automate the processing, microfoundries would ideally carry out selfdirected, multistage processes, involving events that are highly coordinated in both space and time. Here, we use computational modeling to design arrangements of multiple patches of enzymes in a microchamber that drive the localized selfassembly of microparticles, regulate the spatiotemporal motion

of the microparticle assembly, and thereby enable such multistage events. We take advantage of the fact that enzymes (and other catalysts) are only activated by specific reactants; with the introduction of appropriate reactants, the respective enzymatic reaction initiates fluid flow. By tailoring the spatial arrangement of different enzymatic patches (as in Figure 1A-C) and the introduction of reactants at specific times, the spatiotemporal features of the fluid flow can be "patterned" and the system can autonomously transport entire microparticle assemblies among multiple "stations" in the device. In this manner, the chemically generated flow serves as a conveyer belt that delivers this cargo to certain locations, where the particles can undergo further processing. The list and sequence of stations visited by the cargo can be programmed through a sequence of appropriate chemical reactions, which activate the delivery to each station. Importantly, this list and sequence can

Special Issue: Advances in Active Materials

Received: November 14, 2019
Revised: January 23, 2020
Published: February 19, 2020





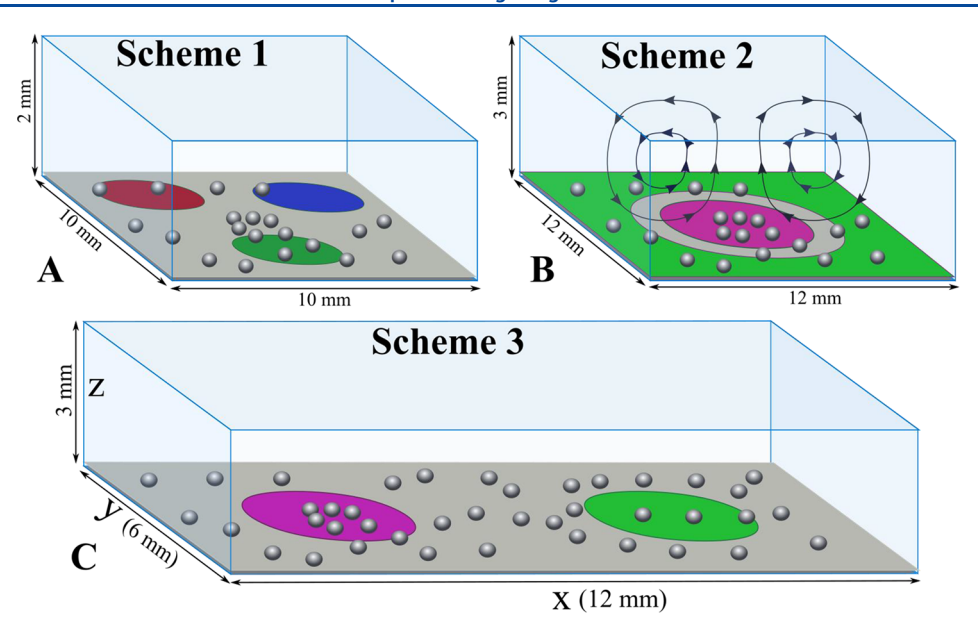


Figure 1. Different arrangements of enzymatic patches used to direct the fluid flow and transport microparticles (gray spheres). Circular patches on the bottom surfaces of the microchambers are coated with different enzymes. (A) Patches are coated with catalase (green), acid-phosphatase (red), and glucose-6-phosphatase (blue). (B, C) Bottom wall is coated with glucose oxidase (magenta) and catalase (green). Addition of appropriate reactants in the solution activates the corresponding enzymatic patches, which in turn produce spontaneous fluid flows (shown by black flow lines in B) and thus, entrain the microparticles.

be readily modified by changing the sequence of reactions. Consequently, the processing operations can be altered by driving the cargo to traverse the stations in a different order.

We note that methods to manipulate the spatiotemporal behavior of microparticles inside fluid-filled chambers can generally be categorized into two groups. The first group of methods utilize external sources of energy to propel the particles along specific directions within a fluid. Examples of this approach include acoustic, amagnetic, and lightdriven 14-16 particle propulsion. A shortcoming of these approaches is that they involve peripheral devices to generate the applied stimuli. Moreover, the particles often need to be modified to be responsive to these stimuli. The second group of methods involve the generation of the fluid flow that transports the particles to the specified location. 1,17 Such convective flows can be generated by the thermal or solutal buoyancy effects that arise from intrinsic chemical reactions occurring within the systems. The advantages of the latter methods are that the particles do not need to be altered and the approach can be applied to both nano- and microscopic particles. Here, we focus on the solutal buoyancy mechanism and show that it provides an effective means of controlling the spatial and temporal trajectories of microparticles within fluidic chambers.

For the systems considered here, the chemically generated fluid flow is due to the effects of solutal buoyancy, which arise from local density variations in the solution. Specifically, if the products of the enzymatic reaction occupy more volume than the initial reactants, the local density of the fluid is decreased, particularly around the enzymatic patch. Consequently, the less dense solution rises upward; this motion is analogous to the less dense fluid rising upward when the bottom of the microchamber is heated. Because the fluid is confined within the chamber, when the upward flow reaches the top of the container, it splits into separate streams that subsequently move downward along the vertical side walls and back toward the enzyme-coated patch. This motion results in the formation

of "inward" convective rolls centered about the patch (Figure 1B). In contrast, if the products occupy less volume than the reactants, the local density around the patch is increased and the more dense fluid flows along the bottom surface, away from the patch. As this confined fluid reaches the upper wall, it forms one central stream that flows downward toward the patch, forming "outward" convective rolls.

In the following studies, we examine three cases that illustrate how the spatial arrangement of the enzymatic patches and time-dependent addition of reactants can be integrated to control the fluid flow and transport of microparticles along specific paths within the microchamber. In the first case (Figure 1A), the surface-anchored patches are arranged in a triangular pattern; with the sequential addition of the appropriate reactants, the microparticles self-organize into aggregates, which move among the patches in a well-defined, controllable manner. In the two other examples, we utilize a cascade reaction (where the products of the first reaction are the reactants for the second) to periodically shuttle a cluster of particles between two enzyme-coated patches. These studies provide a proof-of-concept rather than a comprehensive investigation. Nonetheless, the findings provide valuable design rules for achieving the level of control over particle delivery and localization necessary for ultimately creating effective "microfoundaries" that are driven purely by the inherent transduction of chemical energy into fluid motion and can operate without external mechanical pumps or electronic motors.

#### METHOD

In the presence of j chemical solutes and local temperature T, the local density of the solution can be approximated by  $\rho = \rho_0 \Big( 1 - \beta_T (T - T_0) + \sum_j \beta_j C_j \Big)$ . Here,  $T_0$  is the reference temperature of the solution and  $\rho_0$  is the reference density of the pure solvent. The thermal expansion coefficient of the solvent is  $\beta_T$  (in units of  $K^{-1}$ ), and the solutal expansion

coefficient due to the presence of chemical solute  $C_j$  is  $\beta_j = \frac{1}{\rho_0} \frac{\partial \rho}{\partial C_j}$  (in units of M<sup>-1</sup>). The solutal expansion coefficient reflects the fact that the products of the catalytic reaction can occupy a different volume than the reactants, and thus, the reaction can produce local density variations in the solution.

occupy a different volume than the reactants, and thus, the reaction can produce local density variations in the solution. For the catalytic reactions considered here, these solutal buoyancy effects are significantly greater than the effects due to thermal buoyancy<sup>18</sup> and therefore, the thermal contribution to the flow is ignored.

The density variations within the solution drive the movement of the fluid within the container. Considering that the variations of the density in the solution are relatively small, the fluid motion can be modeled through the Navier–Stokes equation in the Boussinesq approximation. <sup>19</sup> Consequently, the set of equations describing the incompressible fluid are

$$\frac{\partial \mathbf{u}}{\partial t} + (\mathbf{u} \cdot \nabla)\mathbf{u} = -\frac{\nabla p}{\rho_0} + \nu \nabla^2 \mathbf{u} + \frac{\Delta \rho}{\rho_0} \mathbf{g}; \quad \nabla \cdot \mathbf{u} = 0.$$
(1)

Here, p is the isotropic pressure and  ${\bf u}$  denotes the local velocity of the fluid. The kinematic viscosity of the solution is denoted by  $\nu$ , and the vector  ${\bf g}$  accounts for gravity. In addition,  $\Delta \rho = (\rho - \rho_0)$  denotes the difference in the density between the local solution and pure solvent. We utilize no-slip boundary conditions for the fluid on all the walls of the chamber.

The chemical solutes are transported within in the solution by diffusion and the convection of the fluid. The spatial and temporal evolutions for the solutes are modeled by a set of advection-diffusion equations. For solute  $C_p$  the equation is

$$\frac{\partial C_j}{\partial t} + (\mathbf{u} \cdot \nabla)C_j = D_j \nabla^2 C_j; \qquad j \in 1, 2, 3, ...N$$
(2)

The second term on the left side accounts for the advection of solute due to the local fluid velocity,  $\mathbf{u}$ , and the term on the right side of the equation accounts for the diffusive flux.  $D_j$  is the diffusivity of the corresponding solute in the host solvent.

We impose four types of boundary conditions for the solute  $C_j$ . These conditions are (a) no flux of solute through the wall, (b) time-dependent influx of chemical solute, (c) consumption of solute at the enzyme-coated region, and (d) production of solute at the enzyme-coated region. Given that  $\hat{n}$  is the local normal to the surface, the corresponding boundary conditions are

$$D_{j} \frac{\partial C_{j}}{\partial n} = \begin{cases} 0, & \text{(a) no flux} \\ R(t), & \text{(b) chemical influx} \end{cases}$$

$$-\frac{r_{\text{m,region}}^{e} C_{j}}{K_{M} + C_{j}}, & \text{(c) consumption of } C_{j} \\ \text{at enzyme-coated region} \end{cases}$$

$$-\frac{r_{\text{m,region}}^{e} C_{i}}{K_{M} + C_{i}}, & \text{(d) production of } C_{j} \\ \text{at enzyme-coated region} \end{cases}$$

$$\text{at enzyme-coated region} \qquad (3)$$

The catalytic reactions are assumed to follow the Michaelis—Menten kinetics, with  $K_M$  being the Michaelis constant for the corresponding reaction. In case d above,  $C_j$  is the product of a catalytic reaction that depends on the reactant  $C_i$  and the rate of reaction,  $r_{\rm m, region}^{\rm e}$ .

The microparticles immersed in the solution are modeled as spheres of radius a. The density of each sphere is  $\rho_m$ , and each sphere experiences the gravitational force  $\mathbf{F}_g = 4\pi a^3(\rho_m - \rho_0)$   $\mathbf{g}/3$ . Each sphere also experiences steric repulsion from other spheres and the walls of the chamber. The repulsive force between two spheres separated by vector  $\mathbf{r} = \mathbf{r}_j - \mathbf{r}_l$  is  $\mathbf{F}^{ss}(\mathbf{r})$ , where the position vectors of the corresponding spheres are  $\mathbf{r}_j$  and  $\mathbf{r}_l$ . The repulsive force between a sphere and a wall is  $\mathbf{F}^{sw}(\mathbf{r}^w)$ ;  $\mathbf{r}^w$  is the distance between the sphere and nearest point on the respective wall. Both the repulsive forces,  $\mathbf{F}(\mathbf{r}) = -\partial U(r)/\partial \mathbf{r}$ , are modeled through a Morse potential U(r), which is defined as

$$U(r) = \begin{cases} \varepsilon (1 - \exp[-\omega(r - R)])^2, & r < R \\ 0, & r \ge R \end{cases}$$
 (4)

The parameters  $\varepsilon$  and  $\omega$  denote the respective strength and the width of the potential, and R is the equilibrium cutoff distance. Along with the forces described above, the spherical microparticles experience the hydrodynamic drag imparted by the local fluid flow,  $\mathbf{u}(\mathbf{r}_j)$ . Hence, the equation of motion for the particles can be approximated as

$$\frac{\partial \mathbf{r}_{j}}{\partial t} = \mathbf{u}(\mathbf{r}_{j}) + \mu \left( \mathbf{F}_{g} + \sum_{n=1}^{6} \mathbf{F}^{\text{sw}}(\mathbf{r}_{j}^{\text{w}}) + \sum_{l \neq j}^{N} \mathbf{F}^{\text{ss}}(\mathbf{r}_{j} - \mathbf{r}_{l}) \right), \quad 1 \leq j, \quad l \leq N.$$
(5)

Here,  $\mu = \frac{1}{6\pi\eta a}$  is the mobility of a sphere of radius a in a fluid of dynamic viscosity  $\eta = \rho_0 \nu$ .

We numerically solve the governing coupled eqs (eqs 1, 2, and 5) to determine how the motion of the microparticles is affected by varying the spatial placement and temporal activation of the chemical pumps. We employ a single relaxation time Lattice Boltzmann method to solve the Navier—Stokes equation: a finite difference method to solve the advection-diffusion equations and an immersed boundary method to capture the fluid-structure interactions. <sup>20,21</sup> As noted above, we apply no-slip boundary conditions for the fluid at the chamber walls and at the surface of the microparticles. For chemical solutes, the boundary conditions are given by eq 3.

We consider three chambers of different sizes (shown in the Figure 1). The chambers were spatially discretized as a regular grid. The spacing between two consecutive nodes of the grid was  $\Delta x = 200~\mu m$ . To match the kinematic viscosity of the host solution,  $\nu$ , we used the same time-step for each update, which was  $\Delta t = \Delta x^2/6\nu$ . All times mentioned below are obtained by multiplying the time-step with the number of numerical iterations.

A spherical microparticle of radius a is treated as a single node of the immersed boundary method. At each step of a simulation, we interpolate the velocity field and the vorticity field of the fluid at the center of the microparticle, specifically, at  $r_j$  and use the interpolated values to update the position and the orientation of the microparticle. We also prescribe no-slip boundary conditions for the fluid at the bottom surface. Therefore, the microparticle experiences differing drag forces depending on its distance away from the no-slip wall. It also experiences the gradient of flow velocity and shear near the wall.

Additionally, if the center of the microparticle comes closer than its radius, *a*, to a nearby wall, the particle experiences a

repulsive force away from the wall. This force is assumed to act on the center of the specific particle.

The radius of each particle is assumed to be  $a=200~\mu m$ . For this particle size, the effect of Brownian motion is negligible and ignored in the simulation. Also, the frictional force between two microparticles and between the chamber wall and the particle is ignored.

## RESULTS AND DISCUSSION

The self-driven shuttling of cargo between different stations within a microchamber is a vital step within fluidic devices that operate in a self-sustained manner, permitting the device to autonomously perform different analyses at the different stations or coordinate the construction of multicomponent structures (e.g., as in a microfoundry). We devise two different approaches to achieve this self-shuttling within fluid flows driven by the effects of solutal buoyancy. The first approach takes advantage of the specificity of catalytic reactions, which occur only in the presence of appropriate reactants. Hence, the sequential addition of the activating reactant to a chamber containing multiple enzymatic patches allows local control of the flow and thus, local manipulation of particle motion. Figure 1A illustrates how this approach can be utilized with three distinct patches anchored to the bottom wall of a microchamber. The reactant-specific interactions enable the spatially and temporally targeted delivery of microparticles to the desired stations, as detailed below. In the second approach, described further below, we take advantage of catalytic cascades where the addition of just one chemical reactant initiates a chain of interrelated reactions.

A. Sequential Addition of Reactants. The enzymes shown in Figure 1A are chosen so that a particular reactant only activates one of the patches. The green patch represents a region coated with catalase (CAT), the red region is coated with acid phosphatase (AP), and the blue patch is coated with glucose-6-phosphatase (g-6-p). These three enzymes promote three different reactions; catalase converts hydrogen peroxide ( $\rm H_2O_2$ ) to water and oxygen;  $^{22,23}$  AP converts p-nitrophenylphosphate hexahydrate (PNPP) into p-nitrophenol (PNP) and monosodium phosphate ( $\rm NaH_2PO_4$ );  $^{24}$  g-6-p converts glucose-6-phosphate to glucose and phosphate group. In all these reactions, the products are lighter than the reactants.

Figure 2A shows that the microparticles are initially uniformly distributed on the bottom of the chamber, which is decorated with the three enzymes. The sequential addition of reactant through the four side walls of the chamber leads to the dynamic behavior shown in Figure 2B, when hydrogen peroxide is introduced first, followed by PNPP and finally glucose-6-phosphate. Introduction of  $H_2O_2$  activates the CAT pump and thus the fluid undergoes inward flow that is localized around the CAT-coated region (in green). This inward flow in turn drags the particles toward the center of the CAT patch, where they form a distinct cluster (Figure 2B). Ultimately,  $H_2O_2$  is converted to product by the enzymatic reaction and the strength of the fluid flow decreases with the depletion of  $H_2O_2$  in the solution.

With the subsequent introduction of PNPP, the AP-coated region becomes activated and generates an inward flow toward the center of the red patch. The inward flow draws the particles away from the green region and toward the red patch, eventually localizing all the particles in this red region. In effect, the subsequent addition of PNPP enables the controlled

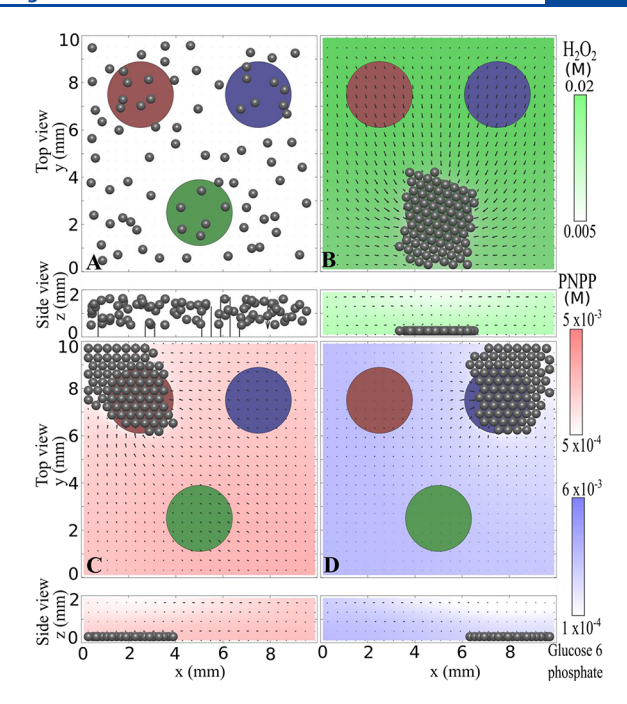


**Figure 2.** Reactant-responsive aggregation of microparticles on top of the patches coated with different enzymes. (A) Initially, the spherical microparticles are dispersed uniformly. (B) Introduction of  $H_2O_2$  in the solution activates the catalase pump (green), which in turn, produces inward convective flows (black arrows) dragging the particles toward the green patch. Sequential introduction of PNPP and glucose-6-phosphate in the solution lead to the corresponding sequential activation of the red and blue patches. Consequently, the particles are dragged by the fluid flow to first move to the red patch (C) and then to the blue patch (D). The background colors show the concentrations of the respective activating reactants. Radius of each patch is 1.4 mm. Reaction rates are  $r_{m, patch}^{ap} = 3 \times 10^{-7} \text{ molm}^{-2} \text{s}^{-1}$ ,  $r_{m, patch}^{cot} = 4.2 \times 10^{-4} \text{ molm}^{-2} \text{s}^{-1}$ ,  $r_{m, patch}^{cop} = 3.5 \times 10^{-7} \text{ molm}^{-2} \text{s}^{-1}$ . The evolution of the particles is presented in SI Video 1.

shuttling of the particles from one patch to another (Figure 2C). Analogous behavior occurs when the majority of PNPP is consumed and glucose-6-phosphate is added to the solution. In particular, the blue g-6-p pumps are activated and the particles are transported toward the blue patch in Figure 2D.

The particle trajectories and the temporal coverage of the different enzymatic patches can be tuned by altering the sequence in which the different reactants are added to the solution. For the example in Figure 3, PNPP is added first, followed by H<sub>2</sub>O<sub>2</sub>, and then glucose-6-phosphate is added last. Consequently, the enzymatic patches are activated in a different order than the example in Figure 2 and the shuttling of the particle follows a different trajectory. Namely, with the sequential activation of the AP (red), CAT (green), and G-6-P (blue) catalysts, the particles move to the respective patches in the corresponding sequence and thus exhibit a counterclockwise trajectory (see Figure 3A-C). The differences between the spatiotemporal trajectories for the examples in Figures 2 and 3 can be quantified by plotting the number of particles on each patch as a function of time. The plot in Figure 3D corresponds to the particle trajectory associated with Figure 2 and shows that the sequential motion of the particles to the respective patches constitutes a clockwise movement, in contrast to the counterclockwise movement (Figure 3E) for the example in Figure 3.

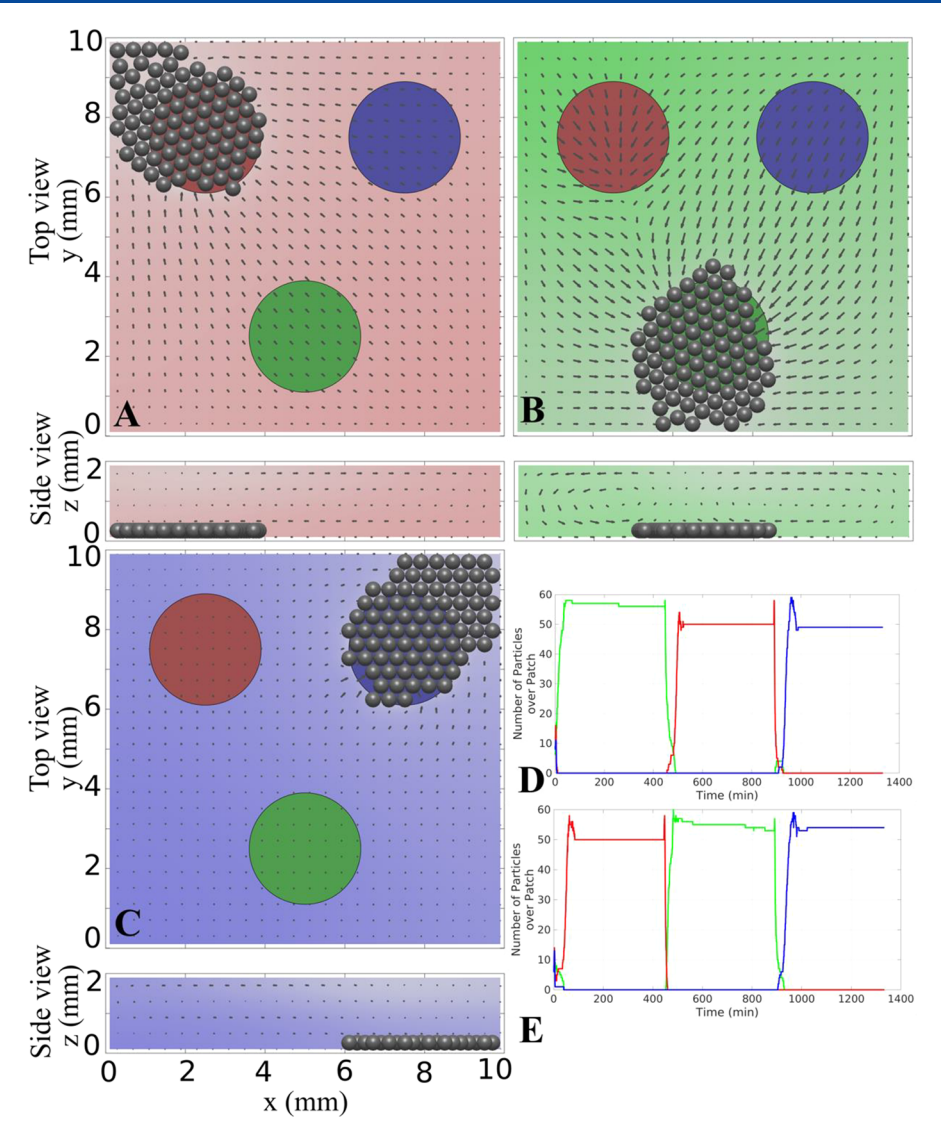


**Figure 3.** Introduction of reactants in a different sequential order provides different spatiotemporal trajectories in a microchamber. In this case, PNPP is introduced first, followed by hydrogen peroxide and glucose-6-phosphate. Consequently, the respective pumps become active sequentially and particles first move to the AP-coated red patch (A), then to the CAT-coated green patch (B), and ultimately to the G-6-P coated blue patch (C). The differences between the particle trajectories are quantified by plotting the number of particles on each patch as a function of time. (D) Particles go from the green patch, to the red, and finally to the blue patch, forming clockwise movement. (E) Particles move from the red patch, to the green patch, and finally to the blue patch forming counterclockwise movement.

The velocity of the transported particles, and hence the speed of the delivery, strongly depends on the particle size. The dependence on particle size arises from the no-slip boundary condition for the fluid at the bottom and top surfaces and the velocity profile produced by an enzymatic patch. Due to the latter influences, the velocity profile across the height of the channel assumes a sigmodal, S-like shape and the horizontal velocity reaches a maximal value at approximately the z = h/4 plane. Therefore, the chamber encompasses a velocity gradient, with zero velocity at the z= 0 plane and the maximum velocity at z = h/4 plane. The fluid drag imposed on the particles by the flows is greater for larger particles and, therefore, provides a shorter transportation time.<sup>26</sup> It is worth noting that thermal buoyancy can also be used to control the motion of microparticles in fluid-filled microchambers. In particular, using UV-light, Tansi et al. 16 heated metallic nanoparticles dispersed throughout the aqueous solution and thereby generated fluid flows to

aggregate and relocate clusters of polystyrene microparticles. For the reactions considered here, however, the typical thermal expansion coefficients (for water,  $\beta_T \sim 10^{-4}~{\rm K}^{-1}$ ) are much smaller than the solutal expansion coefficients ( $\beta_C = 0.01 - 0.1~{\rm M}^{-1}$ ), and hence, the solutal buoyancy mechanism is more effective for the particle transport than the thermal buoyancy effects.

The above studies reveal that the enzymatic pumps and sequential addition of the reactants drive the particles to aggregate within specific regions and permit the staged transport of the assembled aggregate among specific stations. This stepwise movement is important for conducting a specified series of assays and potentially building complex microstructures that depend on the spatially and temporally controlled delivery of cargo. Notably, the path traversed by the particle aggregates can be altered by varying the location of the different patches and the sequence in which the reactants are

added. Furthermore, the cycle can be repeated by addition of fresh reactants.

The time interval between the sequential additions of the reactants is an important factor in achieving this coordinated, collective motion. If the second reactant is introduced before the depletion of the first, then both pumps will be active and compete to drag particles toward the respective catalytic patches. If all the reactants are introduced into the solution simultaneously, all the pumps are activated and will draw cargo particles according to the relative strength of the generated flow (which depends on the amount of reactants added and relative rate constants of the respective reactions). As a result. the particles might divide into separate migrating clusters, with the dynamics being controlled by the amount of reactants, rate constants, and geometries of the enzyme-coated patches. Additionally, if the products of the reactions are not removed from the solution, the solution becomes denser with time. Consequently, the generated fluid velocities and the resulting performance of the transporting cycle might decrease for subsequent repetitions of the cycle.

**B.** Harnessing Cascade Reactions. Another approach for controlling the spatiotemporal delivery of particle aggregates utilizes cascade reactions, where the product of the first reaction is the reactant for the next. To illustrate this scenario, we consider the transport of particles between two catalytic patches; one is coated with glucose oxidase (GOx) and the second is coated with catalase (CAT). With the addition of glucose, the system undergoes a two-step cascade reaction <sup>22,27</sup>

D-glucose + 
$$O_2 \xrightarrow{GOx}$$
 gluconic acid +  $H_2O_2$  (6)

$$2H_2O_2 \xrightarrow{CAT} 2H_2O + O_2 \tag{7}$$

Namely, the D-glucose is consumed to produce H<sub>2</sub>O<sub>2</sub>, which is consumed in the second reaction to produce water and oxygen.

The rate of reaction at the first stage is an order of magnitude slower than the reaction rate at the second stage. Therefore, to increase the effective reaction rate (which is proportional to the area coated with enzyme<sup>28,29</sup>) of the first reaction, we also coat the top walls of the chamber with GOx. The flows generated by the first reaction (eq 6) are qualitatively similar to those depicted in Figure 1B, where the streamlines in the flow field are marked in black, and the arrows indicate that the flow is inward.

The cascade reaction affords new means of controlling the spatiotemporal behavior of the flow since the temporal features of the reactions are innately dependent on sequence. Here, we consider the controlled shuttling of particles between two concentric chemically patterned patches (Figure 1B) as well as two patches at opposite ends of the microchamber (Figure 1C). We first consider the case of two concentric domains (Figure 4A) where the smaller, circular region is coated with GOx (in magenta) and the outer domain (marked in green) is coated with CAT. (The gray region in between these domains is not chemically coated.) The entire structure is located at the bottom wall of the fluid-filled chamber, and glucose is introduced from all the side walls.

With the introduction of glucose, the GOx pump becomes active and generates inward flow because the product of the reaction (hydrogen peroxide) is lighter than glucose. The radially inward flows drag particles toward the GOx patch (Figure 4B). Concomitantly, the increasing concentration of  $H_2O_2$  activates the CAT pump on the outer domain and hence

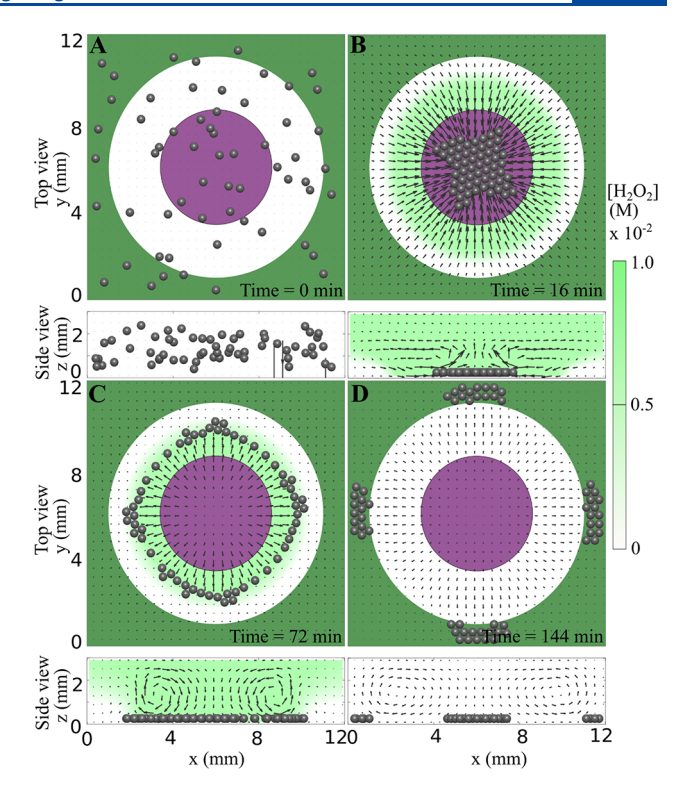


Figure 4. Autonomous particle transport enabled by the cascade reaction. The bottom surface of the chamber is coated with two enzymes: GOx in the circular patch (magenta) at the center and catalase in the outer patch (green). (A) Initially, the cargo particles are distributed uniformly in the solution. (B) Introduction of glucose through all the sidewalls activates the GOx pump, which generates inward fluid flows (black arrows) that assemble cargo particles into a cluster in the center of the patch. Concomitantly, the GOx pump produces a concentration of H<sub>2</sub>O<sub>2</sub> (shown by green color bar) that activates the catalase pump. (C) Consequently, the flow reverses direction and drives the particles radially outward from the central patch. (D) Due to the 4-fold symmetry of the domain, the flows separate particles into four islands near the side walls. The radius of the inner patch is 3.6 mm, and the inner radius of the outer patch is 5.2 mm. Reaction rates are  $r_{\text{m, patch}}^{cat} = 5.4 \times 10^{-4} \text{ mol m}^{-2} \text{s}^{-1}$ ,  $r_{\text{m, patch}}^{gox} = 2.67 \times 10^{-5} \text{ mol m}^{-2} \text{s}^{-1}$ , and  $r_{\text{m, top}}^{gox} = 1.33 \times 10^{-5} \text{ mol m}^{-2} \text{s}^{-1}$ . The evolution of the particles is presented in SI Video 2.

the particles are dragged away from the central GOx patch (Figure 4C). Due to the 4-fold symmetry of the outer CAT domain, the flows pull the particles to the CAT-coated area to form four islands (Figure 4D). The formation of four particle-islands is explained in detail in the Supporting Information (SI). With time, the reactants in the solution become depleted and the fluid stops flowing, leaving the islands of particles intact. The whole cycle of particle movement can be repeated with the periodic introduction of glucose (Figure 5).

The above behavior is quantified through the plots in Figure 5, which shows the salient characteristics of the system when glucose is added periodically to the chamber. The plots reveal the correlations among the following: the concentrations of glucose and hydrogen peroxide, generation of solutal flows, and dynamic behavior of the particles. Due to the two steps in this cascade reaction, the periodic introduction of the glucose (Figure 5A) leads to periodic fluctuations in the concentrations of  $H_2O_2$  in the solution (Figure 5B). The *z*-component of the fluid velocities,  $V_z$ , which is determined at z=1 mm above the central GOx pump, shows the change in the magnitude of the

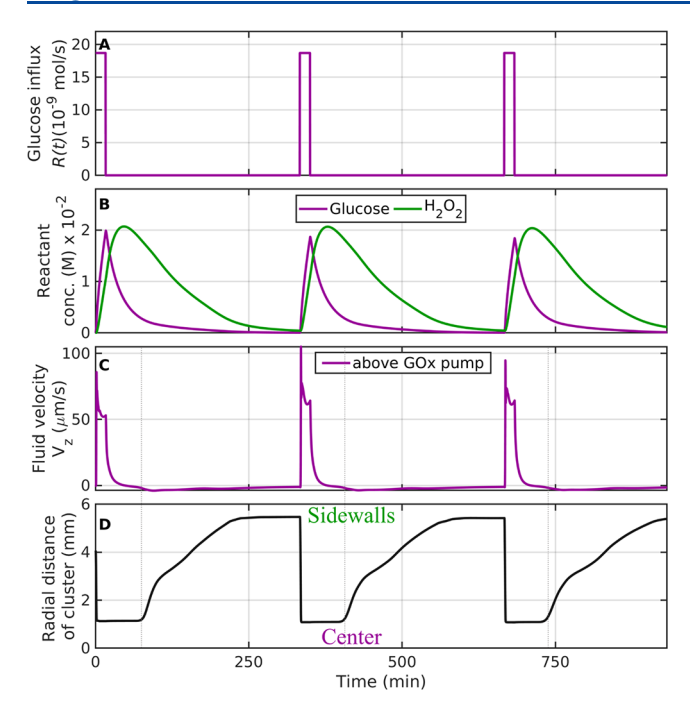
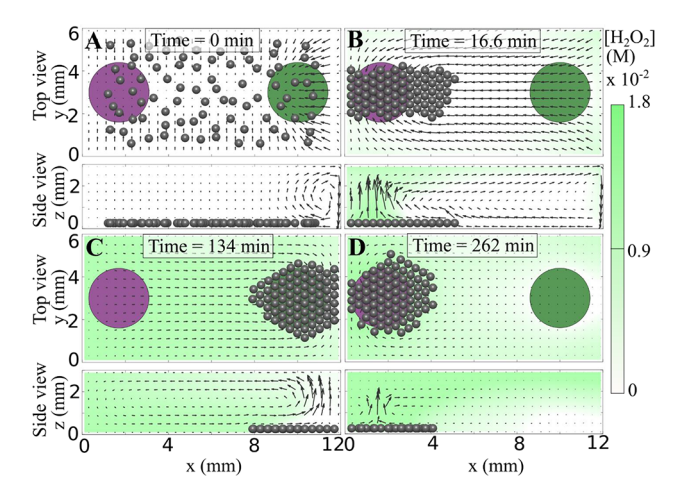


Figure 5. Characteristics of the periodic transport of the particles. (A) Glucose is introduced periodically in the solution, enabling repeatable transport of cargo from the central patch to the outer patch. (B) Variations in the concentrations of glucose and  $\rm H_2O_2$  during the simulation. (C) The vertical component of fluid velocity at 1 mm above the central patch. The direction of flow changes when the catalase pump becomes stronger (i.e., the vertical component of the fluid velocity is greater) than the central GOx pump. (D) The averaged radial distribution of the particles (as a function of the distance from the center of the box) shows the periodic movement of the particles from the center to side walls of microchamber.

flow (Figure 5C) during the course of these periodic changes in the reaction steps. During the first step (eq 6), the flow is dominated by the upward movement of the lighter productrich solution above the central patch, as reflected by the large value of V<sub>2</sub>. During the second stage (eq 7), the glucose is consumed and the inward flow is centered about the outer region, leading to a decrease in  $V_z$  (to approximately zero) about the central GOx-coated patch. In other words, the magnitude of the fluid velocity about the CAT pump is greater than the magnitude at the GOx pump at this stage of the reaction. These spatiotemporal variations in the flow are reflected in the radial distribution function for the particles about the center domain (Figure 5D). In particular, the particles assemble into a single cluster during the first stage of the reaction (Figure 4B) and separate into four smaller clusters located near the side walls during the second stage (Figure 4D).

This single cascade reaction can also be used to shuttle particles between distinct enzyme-coated patches that are separated by a finite distance at the bottom of the chamber (Figure 1C). This shuttling is initiated by the introduction of glucose in the solution through all but the left side walls (see Figure 6A). The introduction of glucose in the solution activates the GOx pump, which generates inward fluid flows that drag the microparticles toward GOx-coated patch (see Figure 6B). The concentration of  $H_2O_2$  in the solution increases due to the first step of the reaction (Figure 6C) and activates the catalase pump. This CAT pump generates flows



**Figure 6.** Periodic transport of particles in a rectangular domain where the bottom surface has two patches coated with enzymes: GOx (magenta) and catalase (green). (A) Introduction of glucose activates the GOx pump and drives fluid flow shown with black arrows. (B) The active GOx pump produces inward fluid flows, which entrain the particles toward the GOx-coated patch. (C) As the concentration of  $H_2O_2$  increases in the solution due to the first reaction, the catalase pump becomes active. Consequently, the particles are pulled by the flow to the catalase pump. (D) A new input of glucose transports the particles to the GOx pump, showing the repeatability of the process. Radius of each patch is 1.4 mm. Reaction rates are,  $r_{m, patch}^{cat} = 2.67 \times 10^{-4} \text{mol m}^{-2} \text{s}^{-1}$ ,  $r_{m, patch}^{gox} = 2.67 \times 10^{-5} \text{ mol m}^{-2} \text{s}^{-1}$ , and  $r_{m, top}^{gox} = 1.33 \times 10^{-5} \text{ mol m}^{-2} \text{s}^{-1}$ . The evolution of the particles is presented in SI Video 3.

with higher velocities than that of the GOx pump and consequently, the flow changes direction along the bottom surface and the fluid moves toward the CAT-coated patch.

This pattern of shuttling can be repeated with the periodic addition of glucose (Figure 7A) and the subsequent periodic production of H<sub>2</sub>O<sub>2</sub> (Figure 7B). A comparison between the dynamic characteristics of the flows generated by the two distinct pumps is shown in Figure 6C, which shows the zcomponent of the fluid velocities,  $V_z$ , measured at z = 1.5 mm above the center of each enzyme-coated patch. The magentacolored peaks in Figure 7C reflect the repeated movement of the cluster from the GOx to the CAT pump (Figure 6C), and the green line reflects the subsequent movements of the cluster back to the GOx region (Figure 6D). This shuttling behavior is also evident from the repeated back and forth motion of the particle cluster along the x-axis of the rectangular channel (Figure 7D). A comparison of Figures 4 and 6 shows that while the concentric circular patches within a square microchamber give rise to the periodic formation of four clusters (Figure 4D) when glucose is added at regular intervals, the arrangement in Figure 6 leads to only one island, which is periodically transported by the flow between the GOx-coated and CATcoated patches.

# CONCLUSIONS

Enzymatic reactions in a fluid-filled microchamber provide a purely chemical means of pumping the fluids within the chamber. In particular, the chemical energy from the reaction is transduced into the mechanical motion of the fluid. We focused on flows driven by the solutal buoyancy mechanism, which arises from the local density variations in the solution produced by the enzymatic reactions. In effect, the system is both self-contained and self-sustained, needing only the

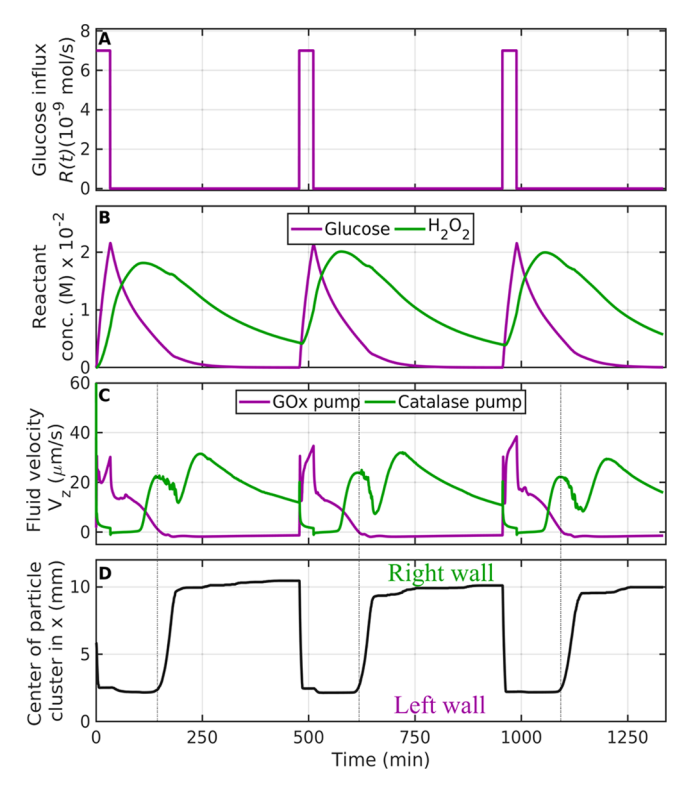


**Figure** 7. Characteristics of periodic transport of particles. (A) Periodic introduction of glucose in the solution. (B) Variations in the concentrations of glucose and  $H_2O_2$  during the simulation. (C) Vertical component of the fluid velocity at z=1.5 mm above two chemical pumps: GOx and CAT. (D) Changes in the *x*-position of the center of the cluster of particles.

addition of reactants to generate and pump flow. Here, we showed that these fluid flows can be spatially "patterned" by varying the arrangement of the enzyme-coated patches on the bottom of the chamber. We also took advantage of the fact that catalysts only react with a specific set of chemicals; in the absence of this "fuel", the catalysts remain inactive. Hence, with multiple, distinct patches, the temporal behavior of the flow can be tailored by adding the appropriate reactants in a specific sequence and time interval. In effect, by varying the spatial configuration of the patches and order in which the reactants are introduced into the chamber, the spatiotemporal behavior of the flow can be finely tuned for performing particular functions.

When microparticles are present in the system, the fluids perform the important function of assembling and then transporting these particles to specified regions and at specific times within a fluidic device. This controlled delivery is important for performing a series of precise assays or assembling multicomponent mixtures into the desired structures. Focusing on three exemplary systems, we showed that the chemically generated and "patterned" flows enabled the particles to be carried along a specified trajectory and delivered to a number of stations in the path of the flow. The number of stations visited along the trajectory can be modified by varying the number of different enzymatic patches (and hence chemical reactions) in the system.

Cascade reactions remove the need for the sequential addition of reactants in order to carry out multistep processes. In this case, each reaction produces the reactants for the next reaction, which enables the delivery of the cargo to the next

location. The number of intermediate steps along the path of particle motion is determined by the number of stages in the reaction cascade.

Overall, the flow-assisted delivery of particles described here acts as a conveyer belt that transports cargo in a self-sustained manner. Both the specific sites and the order of sites to which the cargo is delivered can be programmed by specifying a sequence of chemical reactions, which activate the respective catalytic patches. Such chemically powered and directed conveyor belts can facilitate the development of fluidic devices that autonomously carry out multistage processes.

## ASSOCIATED CONTENT

# Supporting Information

The Supporting Information is available free of charge at https://pubs.acs.org/doi/10.1021/acs.langmuir.9b03546.

Detailed analysis of the formation of four particle-islands in a square domain fueled by a cascade reaction (PDF) Chemically powered conveyer belt. The introduction of

the reactants in a specific order activates appropriate enzymatic patches that lead to the transport of microparticles between different patches (MP4)

Cascade reactions fueling autonomous periodic transport of particles between two concentric enzymatic patches (MP4)

Cascade reactions fueling autonomous periodic transport of particles between two distinct enzymatic patches in a rectangular domain (MP4)

# AUTHOR INFORMATION

# **Corresponding Author**

Anna C. Balazs — Department of Chemical and Petroleum Engineering, University of Pittsburgh, Pittsburgh, Pennsylvania 15261, United States; orcid.org/0000-0002-5555-2692; Email: balazs@pitt.edu

# **Authors**

Abhrajit Laskar — Department of Chemical and Petroleum Engineering, University of Pittsburgh, Pittsburgh, Pennsylvania 15261, United States; orcid.org/0000-0003-2130-5607

Oleg E. Shklyaev – Department of Chemical and Petroleum Engineering, University of Pittsburgh, Pittsburgh, Pennsylvania 15261, United States

Complete contact information is available at: https://pubs.acs.org/10.1021/acs.langmuir.9b03546

#### Notes

The authors declare no competing financial interest.

# ACKNOWLEDGMENTS

A.C.B. gratefully acknowledges funding from NSF Grant 1740630, Centers for Chemical Innovation Phase I, Center for Chemomechanical Assembly and computational facilities at the Center for Research Computing at the University of Pittsburgh.

# REFERENCES

(1) Kline, T. R.; Paxton, W. F.; Wang, Y.; Velegol, D.; Mallouk, T. E.; Sen, A. Catalytic Micropumps: Microscopic Convective Fluid Flow and Pattern Formation. *J. Am. Chem. Soc.* **2005**, *127* (49), 17150–17151.

- (2) Sengupta, S.; Patra, D.; Ortiz-Rivera, I.; Agrawal, A.; Shklyaev, S.; Dey, K. K.; Córdova-Figueroa, U.; Mallouk, T. E.; Sen, A. Self-Powered Enzyme Micropumps. *Nat. Chem.* **2014**, *6* (5), 415–422.
- (3) Sengupta, S.; Spiering, M. M.; Dey, K. K.; Duan, W.; Patra, D.; Butler, P. J.; Astumian, R. D.; Benkovic, S. J.; Sen, A. DNA Polymerase as a Molecular Motor and Pump. *ACS Nano* **2014**, *8* (3), 2410–2418.
- (4) Zhang, H.; Duan, W.; Lu, M.; Zhao, X.; Shklyaev, S.; Liu, L.; Huang, T. J.; Sen, A. Self-Powered Glucose-Responsive Micropumps. *ACS Nano* **2014**, *8* (8), 8537–8542.
- (5) Ortiz-Rivera, I.; Shum, H.; Agrawal, A.; Sen, A.; Balazs, A. C. Convective Flow Reversal in Self-Powered Enzyme Micropumps. *Proc. Natl. Acad. Sci. U. S. A.* **2016**, *113* (10), 2585–2590.
- (6) Das, S.; Shklyaev, O. E.; Altemose, A.; Shum, H.; Ortiz-Rivera, I.; Valdez, L.; Mallouk, T. E.; Balazs, A. C.; Sen, A. Harnessing Catalytic Pumps for Directional Delivery of Microparticles in Microchambers. *Nat. Commun.* **2017**, *8*, 1–10.
- (7) Maiti, S.; Shklyaev, O. E.; Balazs, A. C.; Sen, A. Self-Organization of Fluids in a Multienzymatic Pump System. *Langmuir* **2019**, *35* (10), 3724–3732.
- (8) Gao, W.; Wang, J. Synthetic Micro/Nanomotors in Drug Delivery. *Nanoscale* **2014**, *6* (18), 10486–10494.
- (9) Wang, W.; Castro, L. A.; Hoyos, M.; Mallouk, T. E. Autonomous Motion of Metallic Microrods Propelled by Ultrasound. *ACS Nano* **2012**, *6* (7), 6122–6132.
- (10) Garcia-Gradilla, V.; Orozco, J.; Sattayasamitsathit, S.; Soto, F.; Kuralay, F.; Pourazary, A.; Katzenberg, A.; Gao, W.; Shen, Y.; Wang, J. Functionalized Ultrasound-Propelled Magnetically Guided Nanomotors: Toward Practical Biomedical Applications. *ACS Nano* **2013**, *7* (10), 9232–9240.
- (11) Tierno, P.; Albalat, R.; Sagués, F. Autonomously Moving Catalytic Microellipsoids Dynamically Guided by External Magnetic Fields. *Small* **2010**, *6* (16), 1749–1752.
- (12) Massana-Cid, H.; Martinez-Pedrero, F.; Navarro-Argemí, E.; Pagonabarraga, I.; Tierno, P. Propulsion and Hydrodynamic Particle Transport of Magnetically Twisted Colloidal Ribbons. *New J. Phys.* **2017**, *19* (10), 103031.
- (13) Gao, W.; Kagan, D.; Pak, O. S.; Clawson, C.; Campuzano, S.; Chuluun-Erdene, E.; Shipton, E.; Fullerton, E. E.; Zhang, L.; Lauga, E.; et al. Cargo-Towing Fuel-Free Magnetic Nanoswimmers for Targeted Drug Delivery. *Small* **2012**, *8* (3), 460–467.
- (14) Zhang, Y.; Li, B. Particle Sorting Using a Subwavelength Optical Fiber. Laser Photon. Rev. 2013, 7 (2), 289–296.
- (15) Arzola, A. V; Villasante-Barahona, M.; Volke-Sepúlveda, K.; Jákl, P.; Zemánek, P. Omnidirectional Transport in Fully Reconfigurable Two Dimensional Optical Ratchets. 2017.
- (16) Tansi, B. M.; Peris, M. L.; Shklyaev, O. E.; Balazs, A. C.; Sen, A. Organization of Particle Islands through Light-Powered Fluid Pumping. *Angew. Chem., Int. Ed.* **2019**, *58* (8), 2295–2299.
- (17) Wu, W.-I.; Selvaganapathy, P. R.; Ching, C. Y. Transport of Particles and Microorganisms in Microfluidic Channels Using Rectified Ac Electro-Osmotic Flow. *Biomicrofluidics* **2011**, *5*, 13407.
- (18) Valdez, L.; Shum, H.; Ortiz-Rivera, I.; Balazs, A. C.; Sen, A. Solutal and Thermal Buoyancy Effects in Self-Powered Phosphatase Micropumps. *Soft Matter* **2017**, *13* (15), 2800–2807.
- (19) Chandrasekhar, S. Hydrodynamic and Hydromagnetic Stability; Marshall, W., Wilkinson, D. H., Eds.; Clarendon Press: Oxford, 1961.
- (20) Lim, S.; Ferent, A.; Wang, X. S.; Peskin, C. S. Dynamics of a Closed Rod with Twist and Bend in Fluid. SIAM J. Sci. Comput. 2008, 31 (1), 273–302.
- (21) Shum, H.; Tripathi, A.; Yeomans, J. M.; Balazs, A. C. Active Ciliated Surfaces Expel Model Swimmers. *Langmuir* **2013**, 29 (41), 12770–12776.
- (22) Switala, J.; Loewen, P. C. Diversity of Properties among Catalases. Arch. Biochem. Biophys. 2002, 401 (2), 145–154.
- (23) Gaetani, G.; Ferraris, A.; Rolfo, M.; Mangerini, R.; Arena, S.; Kirkman, H. Predominant Role of Catalase in the Disposal of Hydrogen Peroxide within Human Erythrocytes. *Blood* **1996**, *87* (4), 1595.

- (24) Kruzel, M.; Morawiecka, B. Acid Phosphatase of Potato Tubers (Solanum Tuberisum L.). Purification, Properties, Suger, Amino Acid Composition. *Acta Biochem. Polym.* **1982**, *29*, 321–330.
- (25) van Schaftingen, E.; Gerin, I. The Glucose-6-Phosphatase System. *Biochem. J.* **2002**, 362 (3), 513-532.
- (26) Shklyaev, O. E.; Shum, H.; Yashin, V. V.; Balazs, A. C. Convective Self-Sustained Motion in Mixtures of Chemically Active and Passive Particles. *Langmuir* **2017**, *33* (32), 7873–7880.
- (27) Raba, J.; Mottola, H. A. Glucose Oxidase as an Analytical Reagent. Crit. Rev. Anal. Chem. 1995, 25 (1), 1-42.
- (28) Laskar, A.; Shklyaev, O. E.; Balazs, A. C. Designing Self-Propelled, Chemically Active Sheets: Wrappers, Flappers, and Creepers. Sci. Adv. 2018, 4 (12), eaav1745.
- (29) Laskar, A.; Shklyaev, O. E.; Balazs, A. C.; Weitz, D. A. Collaboration and Competition between Active Sheets for Self-Propelled Particles. *Proc. Natl. Acad. Sci. U. S. A.* **2019**, *116* (19), 9257–9262.